3 Biotech (2018) 8:342
https://doi.org/10.1007/s13205-018-1341-9

ORIGINAL ARTICLE

3D bioprinted rat Schwann cell-laden structures with shape flexibility and enhanced nerve growth factor expression

Xinda Li[1] · Xiong Wang[2] · Xuanzhi Wang[3] · Hongqing Chen[4] · Xinzhi Zhang[1,5] · Lian Zhou[6] · Tao Xu[1,2,7]

Received: 3 April 2018 / Accepted: 6 July 2018 / Published online: 27 July 2018

Abstract

Three-dimensional (3D) bioprinting composite alginate–gelatin hydrogel has encouraged the fabrication of cell-laden functional structures with cells from various tissues. However, reports focusing on printing this hydrogel for nerve tissue research are limited. This study aims at building in vitro Schwann cell 3D microenvironment with customized shapes through 3D bioprinting technology. Rat Schwann cell RSC96s encapsulated in composite alginate–gelatin hydrogel were printed with an extrusion-based bioprinter. Cells maintained high viability of 85.35 ± 6.19% immediately after printing and the printed hydrogel supported long-term Schwann cell proliferation for 2 weeks. Furthermore, after 14 days of culturing, Schwann cells cultured in printed structures maintained viability of 92.34 ± 2.19% and showed enhanced capability of nerve growth factor (NGF) release (142.41 ± 8.99 pg/ml) compared with cells from two-dimensional culture (92.27 ± 9.30 pg/ml). Specific Schwann cell marker S100β was also expressed by cells in printed structures. These printed structures may have the potential to be used as in vitro neurotrophic factor carriers and could be integrated into complex biomimetic artificial structures with the assistance of 3D bioprinting technology.

Keywords Bioprinting · Nerve regeneration · Biomaterial · Neurotrophic factors

Introduction

Schwann cell is a type of glial cell that exists mainly in the peripheral nerve system, and plays an important role in peripheral and even central nerve regeneration (Bunge 1991; Fu and Gordon 1997). On one hand, Schwann cells that form Büngner's bands could guide sprouting axons to the proper sites. On the other hand, as a type of glial cell, Schwann cells also express neurotrophic factors, such as nerve growth factor (NGF), brain-derived nerve growth factor (BDNF), and insulin-like growth factor. These factors are essential for the survival and function of regeneration-related cells (Frostick et al. 1998; Fu and Gordon 1997). Therefore, Schwann cells were seeded in biocompatible polymer nerve conduits or scaffolds to achieve better in vivo nerve regeneration effect and the results of axon growth were comparable with these

✉ Lian Zhou
zlpumch02@163.com

✉ Tao Xu
taoxu@mail.tsinghua.edu.cn

[1] Biomanufacturing and Rapid Forming Technology Key Laboratory of Beijing, Department of Mechanical Engineering, Tsinghua University, Beijing 100084, People's Republic of China

[2] Biomanufacturing Engineering Research Laboratory, Graduate School at Shenzhen Tsinghua University, Shenzhen 518055, People's Republic of China

[3] Department of Neurosurgery, The Second Affiliated Hospital of Soochow University, Suzhou 215004, People's Republic of China

[4] Department of Neurosurgery, Xijing Hospital, Fourth Military Medical University, Xi'an 710032, People's Republic of China

[5] Medprin Biotech GmbH, Gutleutstr 163-167, 60327 Frankfurt, Germany

[6] Department of Stomatology, Peking Union Medical College Hospital, CAMS and PUMC, Beijing 100730, People's Republic of China

[7] Department of Precision Medicine and Healthcare, Tsinghua Berkeley Shenzhen Institute, Shenzhen 518055, People's Republic of China

of autografts (Evans et al. 2002; Gupta et al. 2009; Hadlock et al. 2000; Hurtado et al. 2006; Novikova et al. 2008). Furthermore, Schwann cells also support the growth and have neuro-differentiation effect on stem cells (Krampera et al. 2007; Yi-Hua et al. 2003; Zurita et al. 2005). In these studies, stem cells from different sources showed neural differentiation when co-cultured with Schwann cells. For both in vivo Schwann cell grafts culturing and induction of stem cells by Schwann cells, the number of Schwann cell was regarded as a critical factor on the final effects (Hurtado et al. 2006; Yi-Hua et al. 2003). Thus, scaffolds with sufficient number of Schwann cells will greatly facilitate the nerve regeneration process. Meanwhile, building the proper in vitro microenvironment of Schwann cells which supports Schwann cell proliferation and normal function is also a key issue.

Encapsulating cells in hydrogel scaffolds undoubtedly increases cell number in a single scaffold since cells are evenly distributed in the whole scaffold rather than merely attached on the surface. Suri et al. encapsulated Schwann cells in collagen-hyaluronic hydrogel scaffolds and achieved high cell density. Schwann cells spread and proliferated in the scaffolds. Furthermore, NGF and BDNF were expressed in high quantity when the scaffolds were modified with laminin (Suri and Schmidt 2010). Ning et al. encapsulated Schwann cells in alginate-based hydrogel and found that though Schwann cells did not spread, they survived and proliferated in the hydrogel and Schwann cell function-related proteins were expressed (Ning et al. 2016a). However, in these studies, Schwann cells were encapsulated in bulk hydrogel matrices which may lack channels to achieve substance exchanging. Thus, Schwann cells may not have the optimal microenvironment.

Three-dimensional (3D) bioprinting technology provides a new way to deliver cell-encapsulated hydrogel in pre-defined patterns. Cell-laden structures with high complexity that mimic the geometrical shapes of real tissues or organs can be generated through 3D bioprinting (Melchels et al. 2012; Murphy and Atala 2014). Defined network of channels could also be included in the printed structures for sufficient substance exchange. It could be intuitively imagined that with the aid of 3D bioprinting, Schwann cells will be encapsulated in a hydrogel scaffold that better mimics the native tissue and grow in relatively better microenvironment. Among all the bioprinting methods, extrusion-based bioprinting is widely used for its flexibility in using a wide range of bioinks (Ozbolat and Hospodiuk 2016). Chen's group presented a series of fundamental studies which discussed the effects of encapsulating in hydrogel with different physical properties on Schwann cell viability and proliferation (England et al. 2016; Ning et al. 2016b; Rajaram et al. 2014). Alginate–hyaluronate and fibrin-factor XIII-hyaluronate hydrogel scaffolds were successfully printed (England et al. 2016). While material properties were adjusted by changing the constituent concentration to achieve the best cell viability, these studies did not focus on function, such as NGF release, of Schwann cells.

Alginate or alginate-based hydrogel has already been successfully used for Schwann cell culturing (Mosahebi et al. 2001; Ning et al. 2016b) due to their biocompatibility and extracellular matrix (ECM)-like property, where biocompatibility means cell could survive, proliferate, and function in such materials. Meanwhile, alginate hydrogel is frequently used in bioprinting process due to its easy crosslinking with calcium ions (Hospodiuk et al. 2017). However, alginate or pre-crosslinked alginate is liquid-like and not suitable for direct printing. Gelatin is a denatured form of collagen. When dissolved in water, it forms a solution at physiological temperature (37 °C) and can form a gel when cooled (< 29 °C) (Chung et al. 2013). Therefore, the printability of alginate can be strengthened by incorporating gelatin while retaining the biocompatibility (Chung et al. 2013). Glioma tumor model has been successfully printed with this composite hydrogel in our group (Dai et al. 2016). Taking these into account, we chose composite alginate–gelatin hydrogel as printing material in this study and presumed that Schwann cells would maintain their biological functions in this hydrogel. Moreover, various shapes might also be achieved for the 3D constructs because of the printability of this composite hydrogel.

Although various cells have been printed in alginate–gelatin hydrogel (Ouyang et al. 2015a, b; Zhao et al. 2014), limited researches have focused on printing this hydrogel for neural restoration. Therefore, researches on 3D bioprinting Schwann cells may be a valuable exploration in neural repair. In this study, we aimed at building proper microenvironment for Schwann cells to survive, proliferate, and express relative neurotropic factors. The sufficient space provided by 3D constructs and ECM-like properties of the hydrogel may accommodate large quantities of cells and facilitate the factor expression of Schwann cells for long periods. Furthermore, the printed structures with shape flexibility might also fit the profile of realistic Schwann cell containing tissues, and thus may have the potential to aid in vivo neural restoration. Cells from rat Schwann cell line RSC96 were successfully printed in composite alginate–gelatin hydrogel with extrusion-based bioprinting. The viability, long-term proliferation, and NGF release of RSC96s were examined. The results showed that bioprinted scaffolds contained more cells than two-dimensional culture dish after 2 weeks of culturing. The amount of NGF released by RSC96s in bioprinted scaffolds was also significantly higher than that of 2D cultured cells on day 14.

Materials and methods

Cell culture

RSC96s were purchased from American Type Culture Collection (CRL-2765) and maintained in Dulbecco's Modified Eagle Medium (Gibco, Grand Island, NY, USA, 11965-092) supplemented with 10% fetal bovine serum (Gibco, 10099-141), 100 U/ml penicillin, and 100 µg/ml streptomycin (Gibco, 15140-122). The cells were cultured at 37 °C in a humidified atmosphere. Cells were passaged every 2–3 days.

Material preparation and 3D bioprinting

Sodium alginate (A0682) and gelatin (V900863) powder was purchased from Sigma-Aldrich (St. Louis, MO, USA). The powder was sterilized by gamma ray radiation before use. Sodium alginate and gelatin were dissolved in 0.9% sodium chloride solution at concentrations of 4 and 20% (w/v), respectively.

The printing procedure is shown in Fig. 1. Briefly, for bioprinting, RSC96s were digested and re-suspended in culture medium. The cell suspension was then gently mixed with the alginate–gelatin solution to reach a final concentration of 2% sodium alginate, 10% gelatin, and 2×10^6 cells/ml. The predesigned printing patterns were sliced and transformed into .gcode files by Slic3r (Free access, Alessandro Ranellucci). The .gcode files were then transformed into .cli files which were suitable for the extrusion-based bioprinter (Tissform III, Tsinghua University) with a self-written program. During printing, the cell–hydrogel mixture was loaded into a 1-ml syringe and printing nozzle with an inner diameter of 260 µm (25 gauge) was used considering proper filament diameter and cell viability. The chamber temperature was set at 8 °C and the hydrogel-laden syringe was kept at 37 °C. These parameters were selected to keep gelatin as a liquid before extruding and make it rapidly gelled when deposited on the printing platform. Cells could also sustain high viability while the chamber temperature is 7–10 °C (Ouyang et al. 2015b). Meanwhile, the extrusion speed and nozzle scanning speed were set at 0.15 ml/s and 3.5 mm/s, respectively, for proper deposition of hydrogel filaments. The printed structures were immersed into 3% (w/v) sterilized calcium chloride solution for 3 min for crosslinking.

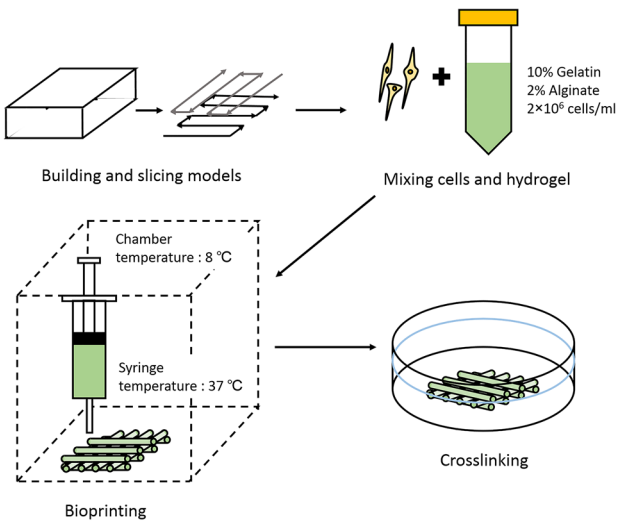

Fig. 1 Schematic demonstration of the printing procedure

Cell viability analysis

Fluorescent live/dead viability assay kit (KeyGEN BioTECH, Nanjing, China, KGAF001) was used to assess cell viability in printed structures following the manufacturer's instruction. Briefly, printed structures were immersed in staining solution containing 8 µM propidium iodide (PI) and 2 µM Calcein-AM. After incubating for 15 min, the structures were washed three times with phosphate buffered saline and observed under fluorescence microscope. Live and dead cells were stained green and red by Calcein-AM and PI, respectively. For cell viability calculation, live and dead cells were counted in ten random sights of magnifying at 100× for each sample ($n = 3$).

Cell proliferation analysis

Alamar Blue Kit (YEASEN, Shanghai, China, 40202ES76) was used to evaluate cell proliferation on days 1, 3, 5, 7, 9, 11, 13, and 15 after printing according to manufacturer's instruction. For proliferation experiment, initial cell number of both 2D and 3D samples was 0.2×10^6. Briefly, Alamar Blue and culture medium were mixed at a ratio of 1:9 to obtain working solution. Samples from each time point ($n = 3$) were incubated with 5 ml working solution for 2 h. The supernatant of each sample was transferred to a 96-well culture plate and its optical density (OD) value was read on a microplate reader (BioTek ELX800, VT, USA) at wavelengths of 570 and 630 nm. The OD values read at 570 mm reflected the actual cell number and those at 630 mm were reference wavelengths which were used for eliminating the effect caused by reagent variation.

Cell morphology

On days 7 and 14 post printing, the printed cell-laden scaffolds were re-crosslinked with 3% calcium chloride for 3 min and fixed for 24 h with 4% paraformaldehyde and embedded with paraffin. The embedded samples were then cut into 4-µm-thick sections for haematoxylin–eosin (HE) staining

to observe cell morphology and tissue formation following the protocol. Images were taken by an optical microscope.

NGF release analysis

Rat NGF enzyme-linked immunosorbent assay (ELISA) Kit (Wuxi Donglin Sci&Tech Development Co. Ltd, Wuxi, China. DL-NGF-Ra) was used to quantify NGF release of 2D and 3D cultured cells at days 4, 7, and 14 according to the manufacturer's protocol. Briefly, the initial cell numbers and the volumes of culture medium of 2D and 3D culturing were controlled to be the same. At each time point, cell culture supernatants were collected and centrifuged at 1000*g* for 20 min. The samples and standards were then incubated in a 96-well ELISA plate coated with anti-NGF antibody for 2 h. After that, detection reagents A and B were successively added and incubated for 1 h, respectively. TMB substrate was added to develop the color and the reaction was stopped by adding stop solution to each well. OD values were read on a microplate reader immediately at the wavelength of 450 nm. The procedure was repeated on days 4, 7, and 14 after printing.

S100β expression

Immunostaining was performed to assess the expression of characteristic protein of RSC96s from cells encapsulated in bioprinted hydrogel scaffolds. Briefly, on day 7 of culturing, the cell-laden scaffolds were re-crosslinked with 3% calcium chloride for 3 min and fixed with 4% paraformaldehyde for 30 min. The scaffolds were then blocked with blocking solution (Beyotime, Shanghai, China, P0260) for 30 min. Anti-S100 beta antibody (Abcam, ab52642) was diluted by primary antibody dilution buffer (Beyotime, Shanghai, China, P0262) at a ratio of 1:100. The scaffolds were submerged in the Anti-S100 beta solution overnight at 4 °C. On the next day, the residual liquid was aspirated and samples were gently washed with normal saline for three times. Secondary antibody (EarthOx, E031240) was diluted by secondary antibody dilution buffer (Beyotime, Shanghai, China, P0265) at a ratio of 1:100. The secondary antibody solution was added and stained for 1 h. After washing with normal saline for another three times, the samples were finally stained with DAPI staining solution for 10 min and images were taken under fluorescence microscope.

Statistical analysis

Each experiment was repeated for three times and the results are presented as mean ± standard deviation. Student's *t* test was used to compare the difference in means between two related groups. $P < 0.05$ was considered statistically significant. All data were analyzed and presented using GraphPad Prism 5 software.

Results

Material printability and RSC96 viability

Figure 2a–c shows several printed structures of this alginate–gelatin hydrogel with different geometrical complexity, including a 'butterfly' structure with the profile of the gray matter in spinal cord. Under the previously set printing condition, the printed structure has a relatively clear marginal edge and 1 mm thickness. Images taken under an optical microscope further showed the printed fibers and grid structures with pores. The material was demonstrated to be printable and the feasibility of the printing procedures was confirmed.

RSC96s in printed alginate–gelatin structures were observed under an optical microscope from day 0 to day 14, as shown in Fig. 2d–f. Cell proliferated in the scaffolds as culture time increased since the scaffolds turned dark and less transparent. It was also noticed that the scaffolds maintained their morphology during culturing period, and the shape of the grid remained identifiable and integrated by day 14 (Fig. 2f). Meanwhile, hydrogel fibers appeared swollen on day 14 when compared with the images taken on day 0 and day 7.

Fluorescent live/dead viability assay kit was used to assess RSC96 viability on day 0 (Fig. 3a–c), day 7 (Fig. 3d–f), and day 14 (Fig. 3g–i) of culturing. Cell viability data were obtained by counting the number of live and dead cells. The viability results on day 0, day 7, and day 14 were 85.35 ± 6.19, 88.88 ± 2.80, and 92.34 ± 2.19%, respectively, as shown in Fig. 3j. There was statistical significance between the data of day 0 and day 14. From the fluorescent images taken on day 0, it could be seen that dead cells distributed along the scaffolds evenly, and no concentrated cell death was observed (Fig. 3a–c).

RSC96 proliferation and NGF release

The proliferation of RSC96s cultured in printed structures was estimated with an Alamar Blue Kit every other day from day 1 to day 15 after printing. RSC96s cultured in 2D petri dishes were used as the control group. A standard curve that describes the relationship between OD values and cell number is presented in Fig. 4a. The OD values shown in Fig. 4b reflect cell proliferation status on each day. It is noticed that 2D cells proliferated faster during initial culturing period and reached the peak on day 5. Then, cell number decreased sharply till day 9, after which the change in cell number became steady. Meanwhile, 3D cultured cells presented an

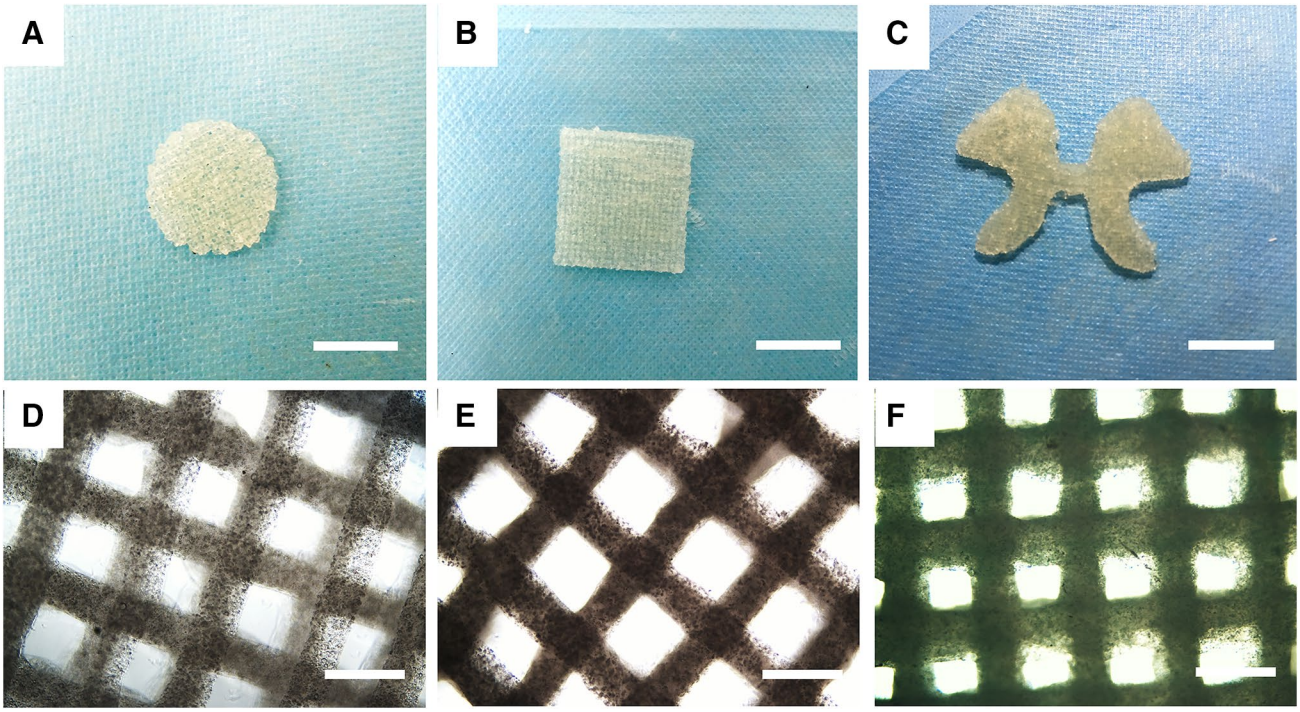

Fig. 2 **a**–**c** Some printed structures with different shapes. Round (**a**), square (**b**), and 'butterfly' (**c**) models with 1 mm thickness. (Scale bar: 1 cm). **d**–**f** Images of printed cell-laden constructs at different culture times under optical microscope. **d** Immediately after printing (day 0), **e** day 7 after printing, **f** day 14 after printing (Scale bar: 200 μm)

overall steadily increasing proliferation portfolio except for day 9 and day 13. At these two time points, cell number appeared to be fewer than that from previous time point. The number of 3D cultured cells first exceeded that of 2D cultured cells at day 9 and the difference remained within a certain range until the end of the experiment.

An ELISA Kit was used to assess release of NGF from 3D and 2D cultured cells and the results are presented in Fig. 5. The test was performed on days 4, 7, and 14 after printing by collecting the spent cell culture medium. The final results were normalized to NGF concentration (pg/ml) released per million cells. In 2D culturing condition, the NGF release results were 43.80 ± 3.50, 43.49 ± 4.62, and 92.27 ± 9.30 pg/ml on days 4, 7, and 14, respectively. The results of 3D cultured cell release were 42.77 ± 14.37, 71.35 ± 6.24, and 142.41 ± 8.99 pg/ml on days 4, 7, and 14, respectively. There is a statistical significance between 3D and 2D cultured results on day 7 and day 14, which demonstrates that NGF released from 3D cultured cells was significantly higher than that from 2D culture when measured at these two time points. Meanwhile, on day 4, no statistical significance was observed. According to Fig. 7, the amounts of NGF released from 3D and 2D cultured cells were approximately at the same level on day 4. NGF released from 3D cultured cells showed an increase on day 7. On the contrary, NGF released from 2D cultured cells remained steady on day 7, while showed an increase on day 14. This finding indicated that the NGF release capability of RSC96s may be enhanced while cultured in printed structures for a long time period.

RSC96 morphology and S100β expression

HE staining images (Fig. 6a–d) show the morphology of RSC96 cells encapsulated in printed alginate–gelatin hydrogel at different time points. Figure 6a, c shows the general distribution of RSC96s in the hydrogel structure on days 7 and 14 post printing, respectively. Structure integrity was roughly maintained and the grids could be identified. It is in accordance with the proliferation curve that the cell number on day 14 was more than that of day 7 when comparing these two images. Figure 6b, d is partially enlarged to show details of printed structures. In addition to the result that cell number increased with the culturing time, it is noticed that proliferated cells were confined by hydrogel and cell aggregates formed during cell proliferation. Cell nuclei were clearly stained in deep purple but little cytoplasm can be seen around the nuclei.

S100β is a typical Schwann cell marker protein which is related to neural cell proliferation and function. This protein is mainly expressed and maintained in cytoplasm. RSC96s were directly stained in printed structures with S100β

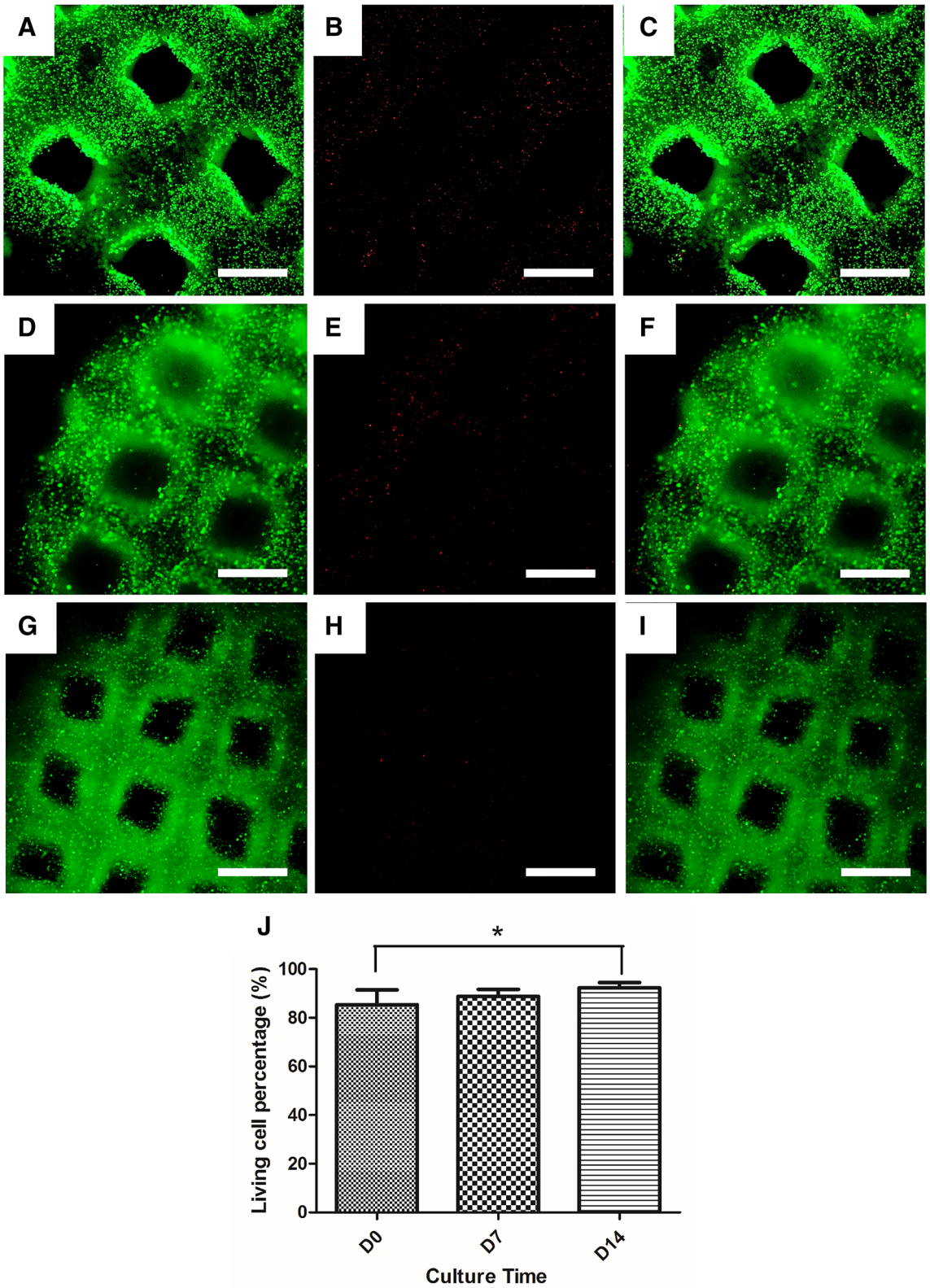

Fig. 3 Live/dead assay results. **a–i** Live cells (**a, d, g**), dead cells (**b, e, h**), and merged images (**c, f, i**) on days 0, 7, and 14 post printing. (Scale bar: 200 µm) **j** cell viability results on days 0, 7, and 14. (*$p < 0.05$)

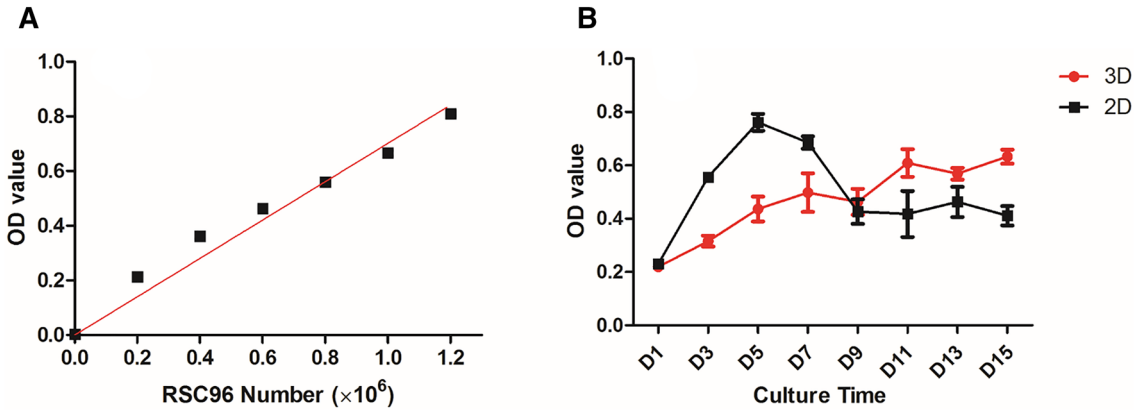

Fig. 4 **a** The standard curve of the performed Alamar Blue Kit. **b** Cell proliferation results from day 1 to day 15

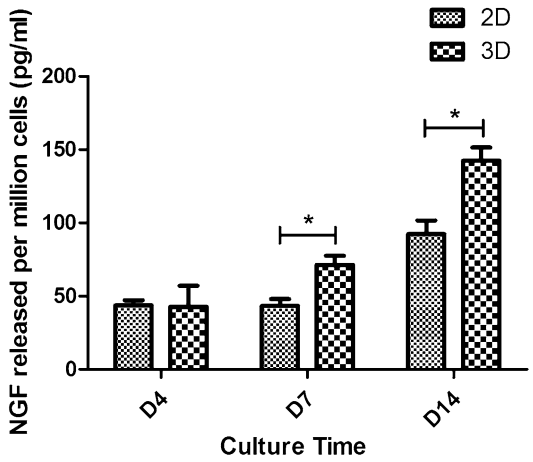

Fig. 5 NGF release of 3D and 2D cultured cells on days 4, 7 and 14 after printing (*$p < 0.05$)

antibodies on day 7 after printing. Results are shown in Fig. 7a–c. According to Fig. 7c, most of the cells expressed S100β, which indicates that printing procedures and 3D culturing did not suppress S100β expression. On the other hand, the green fluorescence also shows the size of cytoplasm of RSC96s. The cytoplasm was in round shape and almost the same size as the nucleus, which could be clearly seen in Fig. 7c. RSC96s also showed no dendrites in 3D hydrogel structures. Briefly, these results collectively indicate that RSC96 did not spread in the hydrogel.

Discussion

Compared with 2D culture dishes, 3D cell-laden hydrogel structures can accommodate more cells and provide more space for cell proliferation, which might further promote a more intense release of protein. With the aid of 3D bioprinting, cell-encapsulated structures will gain more proper geometries and some biomimicry structures could be fabricated with shape accuracy (Fig. 2a–c). Composite alginate–gelatin hydrogel has been widely used to print various kinds of cells including Hela cells, HEK 293FT cells, and embryonic stem cells (Ouyang et al. 2015a, b; Zhao et al. 2014). In these studies, cell survival and function were preserved or even strengthened in the hydrogel compared to 2D culturing condition, because a more biomimic 3D microenvironment was provided. In this study, we first used this composite hydrogel to print Schwann cells RSC96s and evaluated survival, proliferation, morphology and protein expression of these cells in it.

The printed structures sustained their integrity and shape clarity during 14 days of culturing, which is basic for 3D cell culture. As mentioned in the introduction part, gelatin is a thermal-sensitive material which forms a gel below 29 °C and liquefies at 37 °C (Chung et al. 2013). Therefore, degradation of the alginate–gelatin constructs unavoidably occurs in long-term culturing since the culture temperature is 37 °C. Chung et al. indicated a nearly 80% modulus loss in 2% alginate–2% gelatin hydrogel when cultured for 14 days (Chung et al. 2013). In this work, we increased the concentration of gelatin to 10% to strengthen the cell-laden constructs. The cell-laden structures maintained certain mechanical strength for routine operation such as culture media change. However, it should be noticed that the printed structures still became fragile since day 7 of culturing. To overcome this, the structures were re-crosslinked on day 7 to regain sufficient strength for HE staining and immunostaining. Since the requirement on mechanical strength is not high in neural system, with shape flexibility, these structures may act as supporting constructs integrated on other implants to aid neural restoration.

RSC96 viability was 85.35 ± 6.19, 88.88 ± 2.80, and $92.34 \pm 2.19\%$ on day 0, day 7, and day 14 post printing. Cell viability on day 14 was significantly higher than that on day 0. It is possible that the initial cell loss may be due

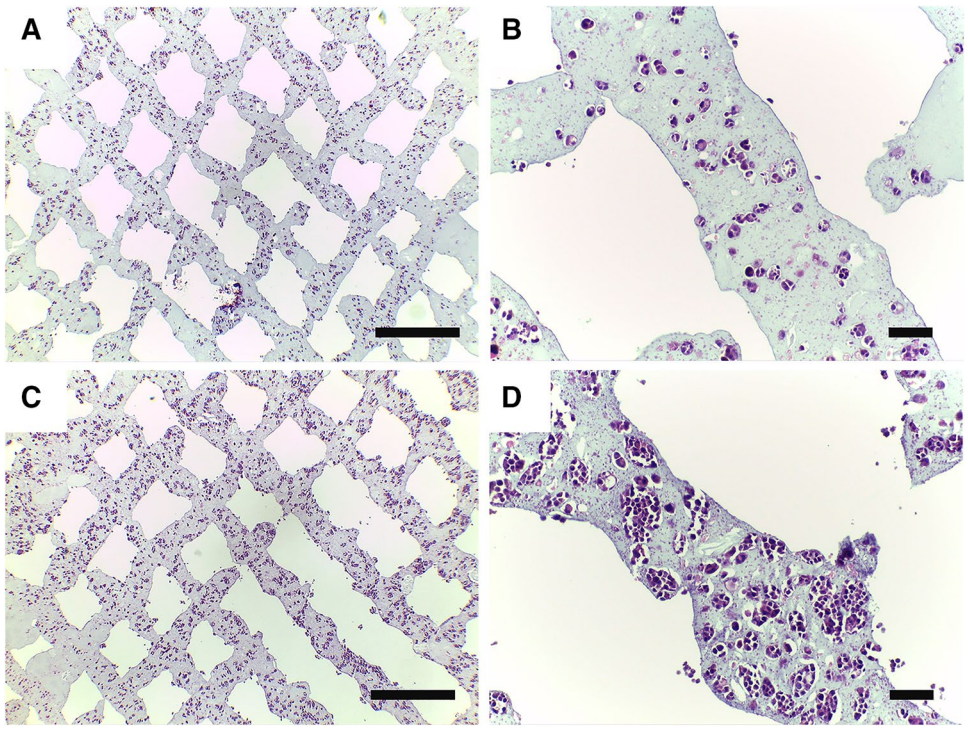

Fig. 6 H&E staining images. **a, b** Cell-laden constructs on day 7 after printing. **c, d** Cell-laden constructs on day 14 after printing (Scale bar: **a, c** 200 µm; **b, d** 50 µm)

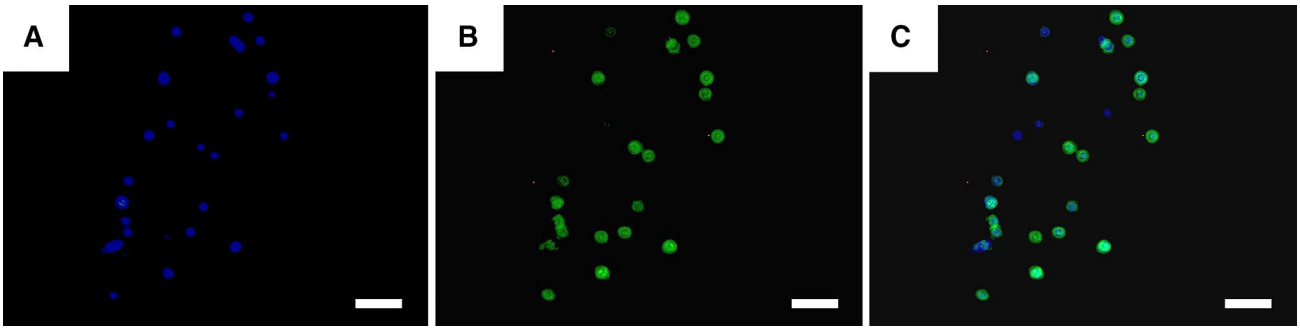

Fig. 7 Immunostaining of S100β Schwann cell marker on day 7. **a** DAPI staining; **b** S100β staining; **c** merged image. (Scale bar: 50 µm)

to the shear stress and relatively low temperature during the extrusion-based bioprinting process (Hospodiuk et al. 2017). As culture time increased, dead cells were gradually lysed and could not be detected by the detecting agent. Meanwhile, cells proliferated in the structures and the proportion of dead cells decreased. RSC96 proliferation in printed scaffolds was further detected with the Alamar Blue Kit and compared to 2D RSC96 proliferation. RSC96s in printed constructs proliferated steadily, while there was a substantial increase in 2D cultured RSC96s during the initial 5 days. Since day 7, the number of 2D cells decreased, which may be due to contact inhibition. This number was finally surpassed by 3D cultured cells on day 9. This result reflects that 3D printed scaffolds have the capability to maintain sufficient cells and support long-term cell proliferation. It is also noticed that reduction in cell number occurred on day 9 and day 13. This can be explained by the loss in gelatin. As mentioned above, gelatin in the composite liquefied at 37 °C and could be partially dissolved in culture medium, which might make a certain amount of cells unstably immobilized and dissociate from the scaffolds. When the number of dissociated cells exceeded the number of proliferated cells, an overall reduction in cell number occurred in 3D structures. Even so, the general tendency of cell proliferation in 3D structures is increasing and the number reached around 0.8×10^6 on day 15.

On the other hand, we have examined NGF release of RSC96s encapsulated in 3D hydrogel scaffolds and cultured in 2D petri dishes. The amount of NGF released from 3D cells was comparable with that of 2D cultured cells on day

4, while significantly higher than that of 2D cultured cells on day 7 and day 14. Since the results were standardized to NGF release of per million cells, it shows that the NGF release capability was strengthened when RSC96s were cultured in the 3D printed composite alginate–gelatin hydrogel during long-term culturing. It is assumed that, on one hand, the RSC96s cultured in 2D dishes had insufficient space to proliferate in the long-term due to contact inhibition, affecting their growing status and NGF release capability, which is also corresponding to the proliferation curve (Fig. 6b) that 2D cell number began to decrease at day 7. For comparison, the stacked cell-laden hydrogel fibers provided more space for 3D cells to proliferate. On the other hand, according to Fig. 6, RSC96s cultured in 3D printed structures proliferated and tightly gathered by day 14. It is also noteworthy that the hydrogel had good deformability to provide space for cells and the cell aggregates had bigger sizes than single cell, and thus were closer to the edge of the scaffolds, which could facilitate substance exchange to deliver more NGF to medium. Furthermore, cell density increased and cell–cell interaction was abundant in these locations, which has been proven to be important factors on regulating Schwann cell gene expression and protein synthesis in previous study (Suri and Schmidt 2010).

Immunostaining of S100β showed that RSC96s retained the ability to express Schwann cell markers. It is also found that no dendrites were developed by RSC96s when cultured in printed alginate–gelatin hydrogel. This may be partially attributed to the lack of the elements for cell attachment in alginate (Hospodiuk et al. 2017; Rowley et al. 1999). Although gelatin includes abundant Arg-Gly-Asp motifs as cell binding cites (Gungorozkerim et al. 2018), we hypothesized that RSC96s did not find gaps to develop dendrites since they were confined in small voids in alginate–gelatin hydrogel. 2% alginate and 10% gelatin were selected to sustain sufficient mechanical strength for long-term cell culture. The selected composite alginate–gelatin hydrogel presented printability, which means proper rheology and gelation rate during printing, as well as maintaining the shape of the printed profiles. However, gelatin at high concentration might strictly confine RSC96s from developing dendrites. In our study, 3D cultured RSC96s with spherical morphology produced NGF higher than 2D cultured RSC96s with normal spread morphology during 14 days of culturing. This amount of NGF was also comparable with NGF released by Schwann cells implanted on surfaces of biomaterials (Yuan et al. 2010). To explain this result, it is hypothesized that RSC96s are mature cell line which have more stable chromosomes than primary Schwann cells extracted from animals, and thus are less likely to reverse to undifferentiated phenotype when in spherical morphology. In addition, since the structures were printed, it was easier for RSC96s encapsulated in thin printed hydrogel fibers to exchange materials with culture medium than that encapsulated in bulk gels because of the enlarged specific surface area in fibers. Thus, 3D printed RSC96s experienced better conditions to survive and proliferate. Moreover, printed RSC96s experienced extrusion process which applied a considerable amount of shear stress on them.

Although NGF were successfully released by spherical RSC96s cultured in printed composite alginate–gelatin hydrogel, a spread cell morphology with dendrites is required for neural regeneration (Behan et al. 2011). Based on the results in this study, composite alginate–gelatin hydrogel is not suitable for dendrite development since the two components were physically mixed and the stiffness might be too high. Adding cell adhesion components (Behan et al. 2011; Li et al. 2016), chemical modification (Hernandez et al. 2016) and alternating the stiffness of hydrogel (Ning et al. 2016a) were demonstrated to be capable of facilitating cell attachment. Therefore, further research will focus on fabricating 3D constructs with these modified hydrogels and gradually promoting the printability of such materials to address the limitation in Schwann cell attachment.

Conclusion

Rat Schwann cell RSC96s encapsulated in alginate–gelatin hydrogel were successfully printed with an extrusion-based bioprinter. The printed hydrogel constructs contained more cells and support long-term cell proliferation compared to 2D culturing conditions. Encapsulated Schwann cells expressed Schwann cell marker and secreted NGF during 1 or 2 weeks of culturing period. The amount of NGF released from printed constructs was higher than that from 2D petri dish cultured cells. This study demonstrates that bioprinted composite alginate–gelatin hydrogel could provide proper microenvironment for Schwann cells and shows a different way to build shape-controllable Schwann cell-encapsulated constructs with enhanced NGF release.

Acknowledgements This work is partly supported by the following programs: Chinese army open Grant (No. BWS17J036); China Shenzhen Peacock Plan Project (No. KQTD201209); and 'Biomanufacturing and Engineering Living Systems' Overseas Expertise Introduction Center for Discipline Innovation (No. G2017002).

Compliance with ethical standards

Conflict of interest The authors declare that they have no conflict of interest.

References

Behan BL, Dewitt DG, Bogdanowicz DR et al (2011) Single-walled carbon nanotubes alter Schwann cell behavior differentially within 2D and 3D environments. J Biomed Mater Res Part A 96:46–57

Bunge RP (1991) Schwann cells in central regeneration. Ann N Y Acad Sci 633:229–233

Chung JY, Naficy S, Yue Z et al (2013) Bio-ink properties and printability for extrusion printing living cells. Biomater Sci 1:763–773

Dai X, Ma C, Lan Q et al (2016) 3D bioprinted glioma stem cells for brain tumor model and applications of drug susceptibility. Biofabrication 8:045005

England S, Rajaram A, Schreyer DJ et al (2016) Bioprinted fibrin-factor XIII-hyaluronate hydrogel scaffolds with encapsulated Schwann cells and their in vitro, characterization for use in nerve regeneration. Bioprinting 5:1–9

Evans GR, Brandt K, Katz S et al (2002) Bioactive poly(L-lactic acid) conduits seeded with Schwann cells or peripheral nerve regeneration. Biomaterials 23:841–848

Frostick SP, Yin Q, Kemp GJ (1998) Schwann cells, neurotrophic factors, and peripheral nerve regeneration. Microsurgery 18:397–405

Fu SY, Gordon T (1997) The cellular and molecular basis of peripheral nerve regeneration. Mol Neurobiol 14:67–116

Gungorozkerim PS, Inci I, Zhang YS et al (2018) Bioinks for 3D bioprinting: an overview. Biomater Sci 6:915–946

Gupta D, Venugopal J, Prabhakaran MP et al (2009) Aligned and random nanofibrous substrate for the in vitro culture of Schwann cells for neural tissue engineering. Acta Biomater 5:2560–2569

Hadlock T, Sundback C, Hunter D et al (2000) A polymer foam conduit seeded with Schwann cells promotes guided peripheral nerve regeneration. Tissue Eng 6:119–127

Hernandez DS, Ritschdorff ET, Seidlits SK et al (2016) Functionalizing micro-3D-printed protein hydrogels for cell adhesion and patterning. J Mater Chem B 4:1818–1826

Hospodiuk M, Dey M, Sosnoski D et al (2017) The bioink: a comprehensive review on bioprintable materials. Biotechnol Adv 35:217–239

Hurtado A, Moon LD, Maquet V et al (2006) Poly (d,l-lactic acid) macroporous guidance scaffolds seeded with Schwann cells genetically modified to secrete a bi-functional neurotrophin implanted in the completely transected adult rat thoracic spinal cord. Biomaterials 27:430–442

Krampera M, Marconi S, Pasini A et al (2007) Induction of neural-like differentiation in human mesenchymal stem cells derived from bone marrow, fat, spleen and thymus. Bone 40:382–390

Li G, Zhao Y, Zhang L et al (2016) Preparation of graphene oxide/polyacrylamide composite hydrogel and its effect on Schwann cells attachment and proliferation. Colloids Surf B Biointerfaces 143:547–556

Melchels FPW, Domingos MAN, Klein TJ et al (2012) Additive manufacturing of tissues and organs. Prog Polym Sci 37:1079–1104

Mosahebi A, Simon M, Wiberg M et al (2001) A novel use of alginate hydrogel as Schwann cell matrix. Res J Appl Sci Eng Technol 7:525–534

Murphy SV, Atala A (2014) 3D bioprinting of tissues and organs. Nat Biotechnol 32:773–785

Ning L, Xu Y, Chen X et al (2016a) Influence of mechanical properties of alginate-based substrates on the performance of Schwann cells in culture. J Biomater Sci Polym Ed 27:898–915

Ning L, Guillemot A, Zhao J et al (2016b) Influence of flow behavior of alginate-cell suspensions on cell viability and proliferation. Tissue Eng Part C Methods 22:652–662

Novikova LN, Pettersson J, Brohlin M et al (2008) Biodegradable poly-β-hydroxybutyrate scaffold seeded with Schwann cells to promote spinal cord repair. Biomaterials 29:1198–1206

Ouyang L, Yao R, Chen X et al (2015a) 3D printing of HEK 293FT cell-laden hydrogel into macroporous constructs with high cell viability and normal biological functions. Biofabrication 7:015010

Ouyang L, Yao R, Mao S et al (2015b) Three-dimensional bioprinting of embryonic stem cells directs highly uniform embryoid body formation. Biofabrication 7:044101

Ozbolat IT, Hospodiuk M (2016) Current advances and future perspectives in extrusion-based bioprinting. Biomaterials 76:321–343

Rajaram A, Schreyer D, Chen D (2014) Alginate/hyaluronic acid hydrogel scaffolds with structural integrity and preserved schwann cell viability. 3d Print Addit Manuf 1:197–203

Rowley JA, Madlambayan G, Mooney DJ (1999) Alginate hydrogels as synthetic extracellular matrix materials. Biomaterials 20:45–53

Suri S, Schmidt CE (2010) Cell-laden hydrogel constructs of hyaluronic acid, collagen, and laminin for neural tissue engineering. Tissue Eng Part A 16:1703–1716

Yi-Hua AN, Wan H, Zhang ZS et al (2003) Effect of rat Schwann cell secretion on proliferation and differentiation of human neural stem cells. Biomed Environ Sci 16:90–94

Yuan Q, Liao D, Yang X et al (2010) Effect of implant surface microtopography on proliferation, neurotrophin secretion, and gene expression of Schwann cells. J Biomed Mater Res Part A 93A:381–388

Zhao Y, Yao R, Ouyang L et al (2014) Three-dimensional printing of Hela cells for cervical tumor model in vitro. Biofabrication 6:035001

Zurita M, Vaquero J, Oya S et al (2005) Schwann cells induce neuronal differentiation of bone marrow stromal cells. Neuroreport 16:505–508